Surface defects repairing of sprayed Ca-P coating by the microwave-hydrothermal method

Yangyang Su[a], Kezhi Li[a,*], Xianghui Hou[b], Song He[a]

[a]*State Key Laboratory of Solidification Processing, Northwestern Polytechnical University, Xi'an 710072, PR China*

[b]*Faculty of Engineering, The University of Nottingham, UK*

Yangyang Su: suyangyang@mail.nwpu.edu.cn

Kezhi Li: likezhi@nwpu.edu.cn (K. -Z. Li) Tel./Fax: +86 29 8849 5764

Xianghui Hou: Xianghui.Hou@nottingham.ac.uk

Song He: 2016200549@mail.nwpu.edu.cn

Abstract

The increasing interest in decreasing the surface defects of sprayed Ca-P coating deposited on carbon/carbon (C/C) composites to enhance the bonding strength, bioactivity and corrosion resistance of the coating is justified by the growing evidence of its beneficial effect on the bone replacement fields. Microwave-hydrothermal (MH) method detailed in the previous study is successfully used to reduce the above coating defects and the MH mechanism is well studied here. Hence, five different treatment reagents involving calcium and phosphorus solution, sulfuric acid (H_2SO_4) solution, ammonium hydroxide ($NH_3 \cdot H_2O$) solution, only Ca^{2+} solution and deionized water are selected as the precursor solution. The surface, cross-sectional morphologies, phase and composition of the coatings are characterized by the scanning electron microscopy (SEM), X-ray diffraction (XRD), Fourier transform infrared spectroscopy (FTIR), microscopy Raman spectroscopy and X-ray photoelectron spectroscopy (XPS) spectra. Elastic modulus and coating hardness are measured by nanoindentation. Results reveal that the presence of calcium and phosphorus ions, as well as the H_2SO_4 in the precursor solution during the MH process, have a positive influence on the reduction of sprayed Ca-P coating surface defects. However, the coating treated by other three solutions cannot produce new phases on the basis of sprayed Ca-P coating and the surface defects of it are not decreased. Nevertheless, the elastic modulus and hardness of the coating treated by H_2SO_4 solution are very weak. MH treated coating by calcium and phosphorus ions in the precursor solution and in $NH_3 \cdot H_2O$ solution, only Ca^{2+} solution and deionized water own the similar elastic modulus and hardness to that of the sprayed Ca-P coating. To conclude, in the MH process, the surface defects of the sprayed Ca-P coating are only lowered in calcium and phosphorus precursor solution and the coating strength is not dropped, which demonstrates the promoting mechanism of MH process.

Keywords: Surface repairing; Sprayed Ca-P coating; Microwave-hydrothermal treatment; Precursor solution; Carbon/carbon composites

1 Introduction

Carbon/carbon (C/C) composites recognized as one of the biomedical materials with unique combination properties for instance low density, excellent mechanical properties, high corrosion resistance and biocompatibility, are widely utilized in bone replacement fields [1-4]. Notably, their elastic moduli are equivalent to that of the human bone. However, numerous carbon particles and fragments released from C/C substrates would be found at the interface while they are directly implanted in the human body [5]. Besides, C/C composites are the biologically inert material with a hydrophobic surface and have no conduction or induction of bone regeneration [6, 7]. Consequently, in order to avoid the generation of carbon fragments and obtain the bioactive substrates, it can be achieved by depositing a C/C substrate with a coating of calcium phosphates [8, 9].

Currently, plasma spray (PS) has proved to be a considerable method for preparing Ca-P coating on the substrate [10]. Among these PS techniques, supersonic atmospheric plasma spray (SAPS) method is commonly considered as one of the ways as it owns the advantages of the environmentally-friendly, good controllability, high efficiency and small thermal damage to the substrates [11, 12]. Generally, in the course of the SAPS process, thermal decomposition and bonding strength of the coating were the main concerns and got full attention as previously reported [13, 14]. Previous researches indicated that sprayed impurity phases consisted of oxy-hydroxyapatite (OHA), tricalcium phosphate (TCP), tetracalcium phosphate (TTCP), calcium oxide (CaO) and dicalcium phosphate anhydrous (DCPA) [14-16]. These impurity phases, as well as the surface defects in the coating, can form mechanically unstable bonds to the bone and diminish the corrosion resistance of the substrate. In present work, fabricated hydroxyapatite ($Ca_{10}(PO_4)_2(OH)_6$, HA) coating is widely applied as the bioactive coating, thanks to its favorable bioactivity and biocompatibility [17-20]. Yang et al. [21] studied the micro-crack changes and phase transition of HA coating after the air calcination and the hydrothermal treatment. The results reflected that the micro-cracks on the coating surface increased after the calcined HA coating for a period, and CaO phase in coating still existed. But when HA coating was treated by hydrothermal method, surface micro-cracks were decreased and impurity phase (CaO) was converted into HA phase. It is indicated that the hydrothermal method can effectively repair the surface defects and homogeneous surface impurities existing in the sprayed HA coating, nevertheless, this process took 6 h and was time-consuming. Li et al. [22] can diminish the impurity phases and the

non-crystalline phases of the sprayed HA coating to achieve the effect of recrystallization by sprayed high-temperature steam for the coating. However, the high-temperature steam equipment is difficult to be controlled during the spraying process and this may lead to the secondary crystallizations. Cao et al. [23] post-processed sprayed HA coating using water vapor method. It is evident that the non-crystalline phase and impurity phase can transform into HA phase, but high-temperature treatment for a long time would cause a certain degree of damage to the HA coating. This is main due to the stress redistribution between the coatings formed and regenerated more secondary micro-cracks. It may reduce the durability of the implant into the human body. Sun et al. [24] used hollow HA powder as the sprayed powder to prepare HA coating. During the spraying process, only using lower spraying power can completely melt HA powder and reduce the thermal decomposition phenomenon of HA phase. Nevertheless, the surface defects appeared in sprayed coating including spherical particles, micro-cracks, holes and un-melted particles are a lack of well studying. In previous work, the related work using microwave-hydrothermal (MH) method to reduce the above defects has been given. MH method is a rapid, simple, environmental-friendly, and it is a promising route to synthesize the crystals on substrates in recent years, such as metals and carbon/carbon (C/C) composites [25, 26]. Meanwhile, microwave heating mainly occurs inside the materials and this heating method makes the materials heat evenly, therefore, having no temperature gradient, stimulating the budding of the crystal, accelerating the rate of the crystallization, lowering the crystallization temperature and shortening crystallization time [27]. Especially, MH treatment without using surfactants, templates, controlling pH values or emulsions, is able to obtain a well-distributed and dense structure [28]. As a result, MH is suggested as a method to repair sprayed Ca-P coating on C/C substrate to achieve the purpose of reducing defects.

To achieve long-term stability of sprayed Ca-P coating, the reduction of the surface defects and impurity phases is the critical factor. Furthermore, MH method is employed, incorporated calcium and phosphorus precursor solution by an in-situ growth of MH treated coating on sprayed Ca-P coating, to suppress the surface defects in coating formation [29]. The uniform morphology appeared on the surface of sprayed Ca-P coating. So far, MH reaction mechanism for using treatment for the repairing to the sprayed Ca-P coating is a lack of study. In this paper, on the basis of MH treated coating fabricated using calcium and phosphorus precursor solution on

sprayed Ca-P coating, H_2SO_4 solution, $NH_3 \cdot H_2O$ solution, only Ca^{2+} solution and deionized water are studied during the MH process to investigate the MH reaction mechanism. For the surface defects in sprayed Ca-P coating, whether MH method plays a role in aqueous of different pH values, only Ca^{2+} solution or in deionized water, the morphology, phases and nanoindentation test are analyzed to justify the result. It is worth noting that only one sprayed Ca-P coating surface is used as the substrate for the subsequent reaction in the MH process. Herein, it is considered that the mechanism of the promoting inhibition in MH route has been determined by the calcium and phosphorus ions in solution.

2 Experimental procedure

2.1 Materials

C/C composites with the density of 1.40 g/cm^3 used in this study, were fabricated through chemical vapor infiltration (CVI) [30]. The preform of the material was two-dimensional needle punched carbon felt (consisting of no weft cloth, a tires layer, and a needle), and the initial density was 0.43 g/cm^3. Subsequently, the mixed natural gas was composed of 96.1% CH_4, 0.45% C_2H_6, 3.2% CO_2, 0.10% other hydrocarbons. A small amount of H_2S and N_2 were used as the precursor. CVI deposition was performed between 900°C ~ 1100°C. C/C substrates were cut into specimens by wire-cutting with the dimension of 8 mm × 8 mm × 2 mm from the bulk. Thanks to the existence of the machine oil and carbon particles on C/C substrates, acetone, ethyl alcohol and deionized water were employed to wash them in an ultrasonic bath, then, dried in an oven for 24 h. The powders for the SAPS process were the commercial HA. Before starting to spray, HA powders were agglomerated to enhance the fluidity. The morphology and phases of the agglomerated HA powders were reported elsewhere [29, 31].

2.2 Deposition of sprayed Ca-P coating on C/C substrate

Sprayed Ca-P coating was manufactured via SAPS technology using HEPJ-100 sprayer on C/C substrate. The detailed parameters for spraying process including voltage, current, carrier gas, a second gas, spraying time, powder feeding rate and specimen position were mentioned in our previous work [29]. Besides, the sprayed Ca-P coating was only produced one surface for the further study. Finally, the obtained sprayed Ca-P coating was cleaned with alcohol to remove the remaining powder on the coating surface for subsequent use.

2.3 MH treatment on sprayed Ca-P coating

MH (MDS-6G, Shanghai, 2450 MHz) as the post process method was carried out on sprayed Ca-P coating. In precursor solution, calcium ions with the concentration of 167 mM were coming from calcium nitrate tetrahydrate ($Ca(NO_3)_2 \cdot 4H_2O$). Ammonium phosphate monobasic ($NH_4H_2PO_4$) was provided as the starting phosphorus ions. The two precursor materials were dissolved in 20 mL of deionized water, respectively. The molar ratio of calcium to phosphorus was 1.67. Then, the resulting solution as well as the specimens were added into a microwave reactor heated to 180°C and maintained at this temperature for 30 min. The MH treated coating could appear on the above sprayed Ca-P coating. The schematic illustration of the composite coating formation on C/C substrate was shown in Fig. 1. Under same MH reaction conditions, H_2SO_4 (98%) solution, $NH_3 \cdot H_2O$ (68%) solution, only Ca^{2+} solution and deionized water solvent were selected as the other four possible treatment reagents to evaluate the MH reaction mechanism [28]. The concentrations of H_2SO_4 solution, $NH_3 \cdot H_2O$ solution and only Ca^{2+} solution with 40 mL of deionized water as the solvent were controlled as follows: 42, 942 and 167 mM according to the literature [32]. The last post-treatment solution in the MH process was only 40 mL of deionized water. Thus, different coatings were prepared from the H_2SO_4 solution, $NH_3 \cdot H_2O$ solution and only Ca^{2+} solution with 40 mL of deionized water and were labeled MH-H-42, MH-OH-942, MH-167, and MH-0, respectively. After that, the specimens were cleaned in deionized water to remove the precipitate remaining on the coating surface, then dried at 60°C for 12 h.

2.4 Characterizations

Surface morphologies of the coatings were carried out using a scanning electron microscopy (Merlin Compact-61-78) with a voltage of 10 kV. The coating surface was sputtered a thin film with gold before testing using ion sputtering apparatus (SBC-12, China). X-ray diffraction (XRD, X'pert Pro MPD) was recorded to analyze the crystalline phases of the coatings using a monochromatized source with Cu Kα generated at 35 mA. Data was collected in the 2θ range of 10°-60°, at a step of 0.03°. Otherwise, the functional groups of the sprayed Ca-P coating, MH treated coating, MH-H-42, MH-OH-167, MH-167, and MH-0 were detected by Fourier transform infrared spectroscopy (Nicolet iS50 FTIR). The molecular structures of the coatings were examined by Raman spectroscopy (Optelics C130) with a 514 nm Ar laser as excitation wavelength. X-ray photoelectron spectroscopy (XPS, Kratos, Manchester) spectra with an Al monochromatized source (1486.6 eV) was used to detect the

elements in the coatings. The binding energy of C1s (284.5 eV) was the standard for calibration of the spectrometer. Nano-Indenter (Agilent U9820A, USA) was employed to evaluate the elastic modulus and hardness of the coatings. Indenter (Berkovich indenter) test depth was 2 μm. 12 indentation points were randomly chosen on the coating. Before testing, the coating surface should be mechanically polished to guarantee the accuracy of the experimental results [33].

3 Results and discussion

3.1 Morphology and phase analysis of the sprayed Ca-P coating

In our previous work, the surface morphologies of sprayed Ca-P coating have been described [25]. In order to expressly understand the typical micrographs of the coating, schematic illustration and the high-resolution micrographs are given in Fig. 2. The main compositions of the sprayed Ca-P coating are clearly depicted as the general plan of defect structure in Fig. 2(a). Naturally, surface defects appeared on the sprayed Ca-P coating mainly include four kinds of morphologies represented in Fig.2(b), (c), (d) and (e). As illustrated, it can be inferred that the spherical particles seem to be caused by the particle impacting on C/C substrate. Consequently, these melted particles are generated splashes. Because of the residual stress in the coating, the micro-cracks will appear when the coating cools to the room temperature. For the holes and un-melted particles forming on C/C substrate, while the hot particles are reached the cold substrate surface, some particles may not be melted before being encountered on the surface of C/C substrate, and some melted particles of HA quickly are solidified.

The XRD results of sprayed Ca-P coating was reported in our previous work [29]. The predominant phase of sprayed Ca-P coating consists of HA, TCP, and CaO. The FTIR spectrum about the sprayed Ca-P coating and its high-resolution scan of the red rectangle block are shown in Fig. 3(a) and (b). As illustrated, all the FTIR characteristic absorption bands of HA and TCP phases can be seen. The peaks appeared around in the 567 cm^{-1}-602 cm^{-1} regions can be related to the v_4 mode of PO_4^{3-}. In addition, the asymmetric stretching vibration of PO_4^{3-} can be observed at around 1040 cm^{-1} and the peaks at 1615 cm^{-1} and 3430 cm^{-1} are assigned as the bending vibration of water. FTIR results are consistent with that of XRD pattern.

3.2 Morphology and phase analysis of MH treated coating

Fig. 4(a) displays the surface morphology of the MH treated coating. It indicates that MH treated coating has a coarse structure mainly composing of the block

particles (Fig. 4b). It is evident that the spherical particles, micro-cracks, holes as well as un-melted particles of sprayed Ca-P coating cannot be observed on the surface of MH treated coating. The XRD pattern, XPS spectra and FTIR spectrum of MH treated coating are depicted in Fig. 4(c), (d), (e) and (f), respectively. As shown in Fig. 4(c), it can be analyzed that the phase of MH treated coating consists of DCPA. Therefore, in comparison to the XRD pattern of sprayed Ca-P coating, the crystalline phase of MH treated coating is enhanced and the HA phase transforms into DCPA with no other foreign phases, implying that sprayed Ca-P coating undergoes chemical reactions during the MH process in calcium and phosphorus precursor solution. From XPS spectra of MH treated coating (Fig. 4d), the chemical composition of the coating is comprised of O1s, Ca2s, Ca2p, C1s, P2s, P2p and Ca3p and they are similar to that of the sprayed Ca-P coating. FTIR spectrum (Fig. 4e and f) also illustrate that MH treated coating comprises hydroxyl vibration (3421 cm^{-1} and 1670 cm^{-1}), PO_4^{3-} (1060 cm^{-1}, 970 cm^{-1} and 565 cm^{-1}) and HPO_4^{2-} (2870 cm^{-1}, 1140 cm^{-1}, 880 cm^{-1} and 535 cm^{-1}), indicating consistent result with the XRD and XPS results.

3.3 Morphology and phase analysis about coatings under different treatments in the MH process

The concentrations of H_2SO_4 solution, $NH_3 \cdot H_2O$ solution and only Ca^{2+} solution during MH reaction process are 42 mM (pH = 1.40), 942 mM (pH = 10.91) and 167 mM, respectively. Furthermore, 40 mL of deionized water is used as the forth treated solvent to evaluate the MH reaction mechanism of the promoting inhibition. SEM micrographs of these four specimens are represented in Fig. 5. From Fig. 5(a), it seems that the surface morphology of the sprayed Ca-P coating has entirely changed in the H_2SO_4 solution (pH = 1.40). Instead of so many defects, uniform rod-like particles appear on sprayed Ca-P coating. Outstandingly, these homogenous structures are formed by the reaction of the H_2SO_4 solution with the sprayed Ca-P coating to consume the original coating, hence, the surface coating under the value of pH = 1.40 becomes loose and compact, and the bonding strength may be lowered. The reason may be that the H_2SO_4 solution reacts with the substances on sprayed Ca-P coating and the crystal particles can grow under the solution that different from the reaction in calcium and phosphorus precursor solution. This new phase formed is a substance to decrease the mechanical properties of sprayed Ca-P coating. The specific reaction may be described as follows:

$$3H_2SO_4 + 3Ca^{2+} \rightarrow 3CaSO_4 + 6H^+ \quad (1)$$

For the MH-OH-942 (Fig. 5b), the surface morphology has few changes except for the blocky-shaped particles appearing around the un-melted particles as shown about yellow arrows in SEM micrographs. However, the defects of the sprayed Ca-P coating also remain. The morphologies of MH-167 is observed in Fig. 5(c). The micro-cracks are also found on the surface of the MH-167 as same as that of the sprayed Ca-P coating. After post treatment with deionized water, the MH-0 is obtained where displays the similar morphologies to MH-OH-942 and MH-167. As a result, the particles on the sprayed Ca-P coating surface could not be controlled to grow into the regular shape in the $NH_3 \cdot H_2O$ solution, only Ca^{2+} solution, and deionized water. The spherical particles, holes and un-melted particles on the coating also appeared on MH-OH-942, MH-167, and MH-0. Meanwhile, the primary micro-cracks as shown in SEM morphologies (yellow arrows) of the coating are also similar to the width of around 2.65 μm, 2.77 μm and 2.64 μm which have basically no changes. The results of these three different cases including $NH_3 \cdot H_2O$ solution, only Ca^{2+} solution, and deionized water are caused because the sprayed Ca-P coating cannot react in the three solutions, indicating that the surface morphologies on sprayed Ca-P coating cannot be occurred great change and reduced the surface defects.

In these four different circumstances, XRD patterns are observed to analyze the phases as depicted in Fig. 6. This confirms that the phase constitutions of the MH-H-42 are $CaSO_4$, dicalcium phosphate dihydrate ($CaHPO_4 \cdot 2H_2O$, DCPD) and TCP. Apparently, HA phase in sprayed Ca-P coating disappeared after post treatment in the H_2SO_4 solution. Noting that the phases in the other three solutions are similar to that of the sprayed Ca-P coating, which is primarily composed of HA and TCP phases. This result illustrates that sprayed Ca-P coating has no chemical reaction with the $NH_3 \cdot H_2O$ solution (pH = 10.91), only Ca^{2+} solution or deionized water. Nevertheless, the sprayed Ca-P coating reacts with the H_2SO_4 solution (pH = 1.40) to get other phases different from the original coating.

The phase mass is given in Fig. 7. RIR method, which is described in the past experimental [34], is utilized to calculate the content in sprayed Ca-P coating, MH treated coating, MH-H-42, MH-OH-942, MH-167, and MH-0, respectively. Noting that the content of CaO in all coatings is not calculated owing to its low content. The sprayed Ca-P coating after post treatment in different solutions consists of HA, TCP, DCPD and $CaSO_4$ phases. From Fig. 7, it can be seen that the HA content appears in the sprayed Ca-P coating, MH-OH-942, MH-167, and MH-0 except for MH treated

coating and MH-H-42, while the phase mass is different from each other. The HA content of MH-OH-942, MH-167, and MH-0 (88%, 91%, and 94%) is higher than that of sprayed Ca-P coating (62%). Most interestingly, while the sprayed Ca-P coating is treated in these solutions ($NH_3 \cdot H_2O$ solution, only Ca^{2+} solution, and deionized water), the HA content has been increasing and the content in MH-0 has the highest HA content. Unfortunately, HA content in MH treated coating and MH-H-42 is 0%. Moreover, HA is replaced by the DCPA (100%), DCPD (42%) and $CaSO_4$ (52%). In contrast, the phases are changed a lot in the MH treated coating and MH-H-42 as a result of the reaction of the sprayed Ca-P coating in the calcium and phosphorus precursor and H_2SO_4 solution.

XPS spectra of MH-H-42, MH-OH-942, MH-167, and MH-0 is shown in Fig. 8(a). The binding energy varies from 0 to 650 eV. It is clear that the chemical composition of MH-H-42 is different from the other coatings (MH-OH-942, MH-167, and MH-0). Compared to the initial composition of O1s, Ca2s, Ca2p, C1s, P2s, P2p and Ca3p correspond to 25 eV, 133 eV, 192 eV, 286 eV, 348 eV, 438 eV and 532 eV, respectively [29]. The S2p and S2s locating at about 170 eV and 234 eV could be observed in the MH-H-42 [35]. Fig. 8(b) ascertains the Raman spectra of the MH-H-42, MH-OH-942, MH-167, and MH-0. The peaks around 437 cm^{-1}, 586 cm^{-1}, 964 $cm^{-1}$and 1048 cm^{-1} are assigned as the typical Raman peaks of PO_4^{3-} which include v_1, v_2, v_3, and v_4. At the same time, the 416 cm^{-1}, 491 cm^{-1}, 616 cm^{-1}, 670 cm^{-1}, 1009 cm^{-1} and 1133 cm^{-1} peaks belong to the SO_4^{2-} groups. Motivated by these results, the chemical compositions of the MH-H-42, MH-OH-942, MH-167, and MH-0 agree well with the XRD results of them. The above results indicate that the sprayed Ca-P coating is favorable for Ca-P nucleation as well as growth in the MH process. Besides, the detailed reaction mechanisms of the coatings are given in Fig. 12(a).

In terms of surface macrocrack of the coating, the sprayed Ca-P coating (in Fig. 9a) has large amounts of macrocracks. Residual stress existing inside the coating after spraying is an important factor to lead to the surface macrocracks. MH treated coating can be observed from Fig. 4(a), and the microcracks are disappeared during MH treatment. Then, the surface macrocracks of MH-H-42, MH-OH-942, MH-167, and MH-0 are changed. In Fig. 9(b), fewer microcracks of MH-H-42 are generated than that of on the sprayed Ca-P coating, forming several holes on the coating surface. About these holes, which are much larger than that of the sprayed Ca-P coating, their appearance may be caused by the coating reaction in solution and the porous nature of

C/C composites. It infers that the macrocracks found in Fig. 5(a) are reduced because of these new morphologies forming on the sprayed Ca-P coating. Additionally, the phase of these morphologies has been shown in XRD patterns that the sprayed Ca-P coating can react with the H_2SO_4 solution. The same phenomenon is observed in Fig. 9(c), (d) and (e). The surface morphologies of the MH-OH-942, MH-167, and MH-0 are still smooth like that of sprayed Ca-P coating. However, these macrocracks can completely be vanished after being treated in the MH process with the calcium and phosphorus precursor solution [29]. The above results demonstrate that the surface defects of the coating are lowered and the holes may still exist in the MH-OH-942, MH-167, and MH-0. It is concluded that the growth of the particles in the sprayed Ca-P coating could expand and fill the macrocracks as well as the holes to achieve the goal. Nevertheless, the growth of particles could not be provided enough ability to repair the surface defects [36]. The macrocracks present in the coating greatly limit the application fields of the coating. In contrast, the MH treated coating not only has the dense structure but also vanishes the surface defects of sprayed Ca-P coating. It is reflected that the repairing defect need not only calcium ions, but also phosphorous ions. Under the circumstances, the calcium ions quickly react with the phosphorous ions forming Ca-P nucleation and then rapid penetration into the coating under the MH process. Although the cracks have few changes after being treated by MH method, in comparison to the high-temperature heat treatments [37, 38], their treatment temperatures are lower and just reach to 180°C, and can achieve the same positive influence as that of the treatment in high temperatures. In addition, some reports about the hydrothermal crystallization on sprayed Ca-P coating are given, however, it would spend much more time than the MH treatment. MH method used in this work could drop the reaction efficiency [21].

The cross-sectional micrographs of the coating reveal the MH repair mechanism (Fig. 10). As expected, for the sprayed Ca-P coating, there are no micro-cracks exist after the MH post treatment. The thickness of MH treated coating is 128.49 ± 1.49 μm, increasing about 33 μm (34.60%) more than that of the sprayed Ca-P coating (95.46 ± 1.36 μm). It indicates that the surface defects of the sprayed Ca-P coating after MH treatment are reduced and generate a new layer on the basis of it. In addition, vast linear structure substances replacing micro-cracks appearing on the sprayed Ca-P coating are illustrated in Fig. 10(b). This result confirms that the original dense sprayed Ca-P coating chemically reacts with the H_2SO_4 solution, and the surface

morphology changes considerably, causing the coating surface to be loose and unstable, which in turn generates big cracks. Additionally, EDS surface map of S element (Fig. 10d) shows that the H_2SO_4 solution is already presented in MH-H-42 which owns the thickness of 184.63 ± 2.34 μm exceeding the sprayed Ca-P coating about 85 μm. It more fully illustrates the chemical reaction of the sprayed Ca-P coating to the H_2SO_4 solution. Obviously, the coating thickness of MH-H-42 increases approximately 89.04%. In Fig. 10(c), (e) and (f), there are still micro-cracks in cross-section of the coating. The cross-sectional morphologies of MH-OH-942, MH-167 and MH-0 are similar to the sprayed Ca-P coating (Fig. 10a), and they possess the coating thicknesses of 93.80 ± 3.21 μm, 98.18 ± 2.03 μm and 99.42 ± 3.25 μm, respectively. Accordingly, the percentages of the corresponding thickness growth increase around -1.74%, 2.85%, and 4.15%, respectively. Importantly, the results illustrate that the coating thickness is similar to that of the sprayed Ca-P coating. It infers that the coating surface may not have a chemical reaction after MH post treatment. On the other hand, the coating thickness of these three specimens (MH-OH-942, MH- 167, and MH-0) is greatly related to the properties of the precursor solution during the MH treatment.

The curves in Fig. 11 are the nanoindentation results (load-displacement) of the MH treated coating, MH-H-42, MH-OH-942, MH-167, and MH-0, respectively. The corresponding elastic modulus and coating hardness are listed in Table 1. Combining the load-displacement curve with the Table 1 and its curve change (Fig.12), the conclusions are summarized as follows: (1) compared to the elastic modulus and hardness (57.5 ± 16.5 GPa and 3.20 ± 1.11 GPa) of sprayed Ca-P coating, MH treated coating, MH-OH-942, MH-167, and MH-0's don't change largely. Among them, the little increase in the strength of MH treated coating is mainly owing to the fact that a new layer is produced on the sprayed Ca-P coating. The result leads to the enhancement of the coating strength while repairing the surface defects of the sprayed Ca-P coating. Regarding to the MH-OH-942, MH-167, and MH-0, a slight decreased strength occurs because of the lack of new layers on the sprayed Ca-P coating surface after MH treatment. In this case, the surface defects of the MH-OH-942, MH-167, and MH-0 have not been reduced. The reason is main that the specimens move back and forth while the solution is boiling in the reaction vessel during the reaction process, therefore, the strength of the original basis coating is decreased; (2) especially, for MH-H-42, its elastic modulus and hardness are very small, and it is able to be seen

from the curve that coating strength is deemed to a straight line, which indicates that the strength of sprayed Ca-P coating treated by H_2SO_4 solution is inferior. It indicates the chemical reaction happens on the sprayed Ca-P coating in H_2SO_4 solution, which transforms the original dense coating from calcium and phosphorus to the calcium sulfide as seen from XRD pattern in Fig. 6. Finally, a loose porous coating appears, namely, MH-H-42.

The coating formation mechanism of promoting inhibition in the MH process is concluded as the following three reasons: Firstly, there are amounts of reactive activation points on the surface of the sprayed Ca-P coating while it is post-processed in the calcium and phosphorus precursor solution. This situation is more likely to activate the reaction for the MH post treatment. Secondly, other impurity phases in the sprayed Ca-P coating, such as TCP, can react with water to provide the reaction conditions. The possible equations of reaction are shown as follows:

$$PO_4^{3-} + H_2O \rightarrow HPO_4^{2-} + OH^- \quad (1)$$

$$HPO_4^{2-} + H_2O \rightarrow H_2PO_4^{1-} + OH^- \quad (2)$$

Thirdly, HA phase in the sprayed Ca-P coating has much rich hydroxy when the MH process is carried out in an aqueous environment. Consequently, the Ca^{2+} can be concentration on the sprayed Ca-P coating and instantaneously saturate to form a Ca-P nucleation to generate the new layer. Next, it is schematically described the possible reactions and mechanism of the MH treated coating, MH-H-42, MH-OH-942, MH-167 and MH-0. As it is seen from Fig. 13, the detailed mechanism for the formation of products in the MH process is described. In the stage of forming MH treated coating, calcium and phosphorus precursor solution, which has a Ca-P molar ratio of 1.67, promotes the formation of the new layer and reduces the surface defects of sprayed Ca-P coating. The mechanism for defect repairing of sprayed Ca-P coating is reported in our previous work [29]. MH-H-42 is the reaction product of the sprayed Ca-P coating and H_2SO_4 solution. It is evident that sprayed Ca-P coating can be easily dissolved in the H_2SO_4 solution and a new loose layer appears on the sprayed Ca-P coating. Nevertheless, this circumstance implies that the sprayed Ca-P coating is unstable in the H_2SO_4 solution which may lead to surface relaxation and damage the surface stability although there are no surface defects on MH-H-42. Furthermore, the mechanisms for the MH-OH-942, MH-167, and MH-0 are basically identical which are concluded that the sprayed Ca-P coating cannot react with the $NH_3 \cdot H_2O$ solution, only Ca^{2+} solution, and deionized water. This confirms that the surface defects of the

sprayed Ca-P coating cannot be repaired in $NH_3 \cdot H_2O$ solution, only Ca^{2+} solution, and deionized water, respectively during the MH process. But a small number of (calcium and phosphorous) ions from precursor solution have a critical role in the repairing surface defects of sprayed Ca-P coating by the microwave-hydrothermal method.

Conclusions

Sprayed Ca-P coating is post-processed by the MH method to lower the surface defects (spherical particles, micro-cracks, holes and un-melted particles). The promotion inhibition of the MH process under different conditions is investigated. The main conclusions are as follows:

(1) Surface morphologies of the coatings including the sprayed Ca-P coating, MH treated coating, MH-H-42, MH-OH-942, MH-167 and MH-0 indicate that the MH postprocessing with calcium and phosphorus ions can accelerate the apatite coating formation with the high molar ratio of Ca/P (1.67). Nevertheless, the reason for the substantial changes of morphology for MH-H-42 is that the H_2SO_4 solution reacts with the sprayed Ca-P coating. Furthermore, for MH-OH-942, MH-167, and MH-0, there are no visible morphology changes which dramatically demonstrates the MH reaction mechanism of promoting inhibition and the surface defects of sprayed Ca-P coating are unchanged.

(2) From the XRD patterns, XPS spectra, FTIR spectrum as well as Raman spectra, it can be concluded that the coating phases consist of HA and TCP in the course of the different MH process ($NH_3 \cdot H_2O$ solution, only Ca^{2+} solution, and deionized water). Except for that, the crystalline phases comprised of HA, TCP, DCPA, DCPD and $CaSO_4$ appeared in MH treated coating and MH-H-42, respectively, which are different from the coatings as the above mentioned. It is noted that DCPA phase of MH treated coating is formed and decreases the surface defects of the sprayed Ca-P coating, but the DCPD and $CaSO_4$ phases appear in the MH-H-42 due to the reaction in solution with the H_2SO_4 solution. Although this process also diminishes the surface defects forming on the sprayed Ca-P coating, the surface shows the loose structure, which is not the positive effect of calcium and phosphorous ions in the MH process.

(3) Nanoindentation results illustrate that the sprayed Ca-P coating under the calcium and phosphorus precursor, $NH_3 \cdot H_2O$ solution, only Ca^{2+} solution and deionized water treatment during the MH process has the similar elastic modulus and hardness. But the coating is treated in the H_2SO_4 solution, the strength of the coating

decreases about 97.39% and 99.69% for elastic modulus and hardness, respectively. Therefore, MH treated coating, namely post-processed in the calcium phosphorus precursor solution, can repair the surface defects of sprayed Ca-P coating and owns the good coating strength.

Acknowledgments

This work was supported by the National Natural Science Foundation of China under Grant No.51521061 and 51727804, the Fundamental Research Funds for the Central Universities (No. 3102014JCQ01030), the Research Fund of the State Key Laboratory of Solidification Processing (NWPU), China (Grant No. 136-QP-2015) and "111" project of China (B08040).

References

[1] C. Baquey, L. Bordenave, N. More, J. Caix, B. Basse-Cathalinat, Biocompatibility of carbon-carbon materials: Blood tolerability, Biomaterials, 10 (1989) 435-440.

[2] L. Zhang, L. Pei, H. Li, S. Li, S. Liu, Y. Guo, Preparation and characterization of Na and F co-doped hydroxyapatite coating reinforced by carbon nanotubes and SiC nanoparticles, Materials Letters, 218 (2018) 161-164.

[3] C. Sheng, H. Li, J. Lu, L. Zhang, Unique cytological behavior of MC3T3-E1 osteoblasts on H_2O_2-modified C/C composites in vitro, Science China Materials 60(4) (2017) 361-367.

[4] Y. Guo, L. Zhang, H. Li, S. He, X. Tian, H. Sheng, Q. Song, Microstructure and interlaminar shear property of carbon fiber-SiC nanowire/pyrolytic carbon composites with SiC nanowires growing at different positions, Ceramics International, (2018).

[5] L. Bacáková, V. Starý, O. Kofronová, V. Lisá, Polishing and coating carbon fiber-reinforced carbon composites with a carbon-titanium layer enhances adhesion and growth of osteoblast-like MG63 cells and vascular smooth muscle cells in vitro, Journal of Biomedical Materials Research Part A, 54 (2001) 567.

[6] X. Zhao, T. Hu, H. Li, M. Chen, S. Cao, L. Zhang, X. Hou, Electrochemically assisted co-deposition of calcium phosphate/collagen coatings on carbon/carbon composites, Applied Surface Science, 257 (2011) 3612-3619.

[7] Z. Leilei, L. Wei, L. Hejun, L. Shoujie, L. Shaoxian, Z. Yulei, Formation of dicalcium phosphate dehydrate coating on carbon fibers with in-situ grown graphene nanosheet interlayer, Ceramics International, 43 (2017) 5968-5973.

[8] N. Cao, J. Dong, Q. Wang, Q. Ma, C. Xue, M. Li, An experimental bone defect healing with hydroxyapatite coating plasma sprayed on carbon/carbon composite

implants, Surface & Coatings Technology, 205 (2010) 1150-1156.

[9] G.L. Maistrelli, N. Mahomed, D. Garbuz, V. Fornasier, I.J. Harrington, A. Binnington, Hydroxyapatite coating on carbon composite hip implants in dogs, Journal of Bone & Joint Surgery British Volume, 74 (1992) 452-456.

[10] J. Cizek, K.A. Khor, Role of in-flight temperature and velocity of powder particles on plasma sprayed hydroxyapatite coating characteristics, Surface and Coatings Technology, 206 (2012) 2181-2191.

[11] Y. Jia, H. Li, Q. Fu, Z. Zhao, J. Sun, Ablation resistance of supersonic-atmosphere-plasma-spraying ZrC coating doped with ZrO_2 for SiC-coated carbon/carbon composites, Corrosion Science, 123 (2017) 40-54.

[12] L. Wang, Q.G. Fu, F.L. Zhao, A novel gradient SiC-ZrB_2 -$MoSi_2$ coating for SiC coated C/C composites by supersonic plasma spraying, Surface & Coatings Technology, 313 (2017) 63-72.

[13] H. Daugaard, B. Elmengaard, J.E. Bechtold, T. Jensen, K. Soballe, The effect on bone growth enhancement of implant coatings with hydroxyapatite and collagen deposited electrochemically and by plasma spray, Journal of Biomedical Materials Research Part A, 92A (2010) 913-921.

[14] J.L. Sui, M.S. Li, Y.P. Lu, Y.Q. Bai, The effect of plasma spraying power on the structure and mechanical properties of hydroxyapatite deposited onto carbon/carbon composites, Surface and Coatings Technology, 190 (2005) 287-292.

[15] J.C. Knowles, K. Gross, C.C. Berndt, W. Bonfield, Structural changes of thermally sprayed hydroxyapatite investigated by Rietveld analysis, 17 (1996) 639-645.

[16] M.T. Carayon, J.L. Lacout, Study of the Ca/P atomic ratio of the amorphous phase in plasma-sprayed hydroxyapatite coatings, Journal of Solid State Chemistry, 172 (2003) 339-350.

[17] Y. Huang, L. Song, X. Liu, Y. Xiao, Y. Wu, J. Chen, F. Wu, Z. Gu, Hydroxyapatite coatings deposited by liquid precursor plasma spraying: controlled dense and porous microstructures and osteoblastic cell responses, Biofabrication, 2 (2010) 045003.

[18] L. Zhang, H. Li, S. Liu, S. Li, L. Pei, Y. Guo, Y. Zhang, In situ grown Si3N4 microbelt/Mg doped hydroxyapatite dual-layer coating on carbon/carbon composites for biomedical application, Materials Letters, 194 (2017) 70-73.

[19] L. Zhang, S. Li, H. Li, L. Pei, Bioactive surface modification of carbon/carbon

composites with multilayer SiC-SiC nanowire-Si doped hydroxyapatite coating, Journal of Alloys & Compounds, 740 (2017).

[20] L. Zhang, H. Li, Y. Zhao, B. Li, F. Ren, M. Chang, Y. Zhang, Corrosion behavior of SiC-hyaluronic acid-Sr doped dicalcium phosphate dihydrate composite coating in simulated body fluid, Ceramics International, 43 (2016).

[21] C.W. Yang, T.S. Lui, L.H. Chen, Hydrothermal crystallization effect on the improvement of erosion resistance and reliability of plasma-sprayed hydroxyapatite coatings, Thin Solid Films, 517 (2009) 5380-5385.

[22] H. Li, K.A. Khor, P. Cheang, Effect of steam treatment during plasma spraying on the microstructure of hydroxyapatite splats and coatings, Journal of Thermal Spray Technology, 15 (2006) 610-616.

[23] Y. Cao, J. Weng, J. Chen, J. Feng, Z. Yang, X. Zhang, Water vapour-treated hydroxyapatite coatings after plasma spraying and their characteristics, Biomaterials, 17 (1996) 419.

[24] R. Sun, Y. Lu, K. Chen, Preparation and characterization of hollow hydroxyapatite microspheres by spray drying method, Materials Science & Engineering C, 29 (2009) 1088-1092.

[25] Y. Su, K. Li, L. Zhang, S. Liu, Y. Yuan, S. He, Calcium phosphorus bio-coating on carbon/carbon composites: Preparation, shear strength and bioactivity, Applied Surface Science, 419 (2017) 503-511.

[26] J. Zhang, X. Wang, X. Zhang, X. Zhao, X. Liu, L. Peng, Microwave synthesis of $NaLa(MoO_4)_2$ microcrystals and their near-infrared luminescent properties with lanthanide ion doping (Er^{3+}, Nd^{3+}, Yb^{3+}), Inorganic Chemistry Communications, 14 (2011) 1723-1727.

[27] J.S. Schanche, Microwave synthesis solutions from personal chemistry, Molecular Diversity, 7 (2003) 291-298.

[28] X. Zhang, B. Li, C. Liu, Q. Chu, F. Liu, X. Wang, H. Chen, X. Liu, Rapid microwave-assisted hydrothermal synthesis of morphology-tuned MnO_2 nanocrystals and their electrocatalytic activities for oxygen reduction, Materials Research Bulletin, 48 (2013) 2696-2701.

[29] Y. Su, K. Li, L. Zhang, J. Sun, S. Liu, G. Liu, Effect of microwave heating time on bonding strength and corrosion resistance of Ca-P composite layers for carbon/carbon composites, Journal of Alloys and Compounds, 713 (2017) 266-279.

[30] H. Deng, K. Li, H. Li, X. Li, L. Zhang, W. Cao, Densification behavior and

microstructure of carbon/carbon composites prepared by chemical vapor infiltration from xylene at temperatures between 900 and 1250 °C, Carbon, 49 (2011) 2561-2570.
[31] Y. Su, K. Li, L. Zhang, S. Farhan, S. Liu, G. Shi, Ca-P bioactive coating prepared by combining microwave-hydrothermal and supersonic atmospheric plasma spraying methods, Mater Sci Eng C Mater Biol Appl, 72 (2017) 371-377.
[32] X. Zhang, B. Li, C. Liu, Q. Chu, F. Liu, X. Wang, H. Chen, X. Liu, Rapid microwave-assisted hydrothermal synthesis of morphology-tuned MnO 2 nanocrystals and their electrocatalytic activities for oxygen reduction, Materials Research Bulletin, 48 (2013) 2696-2701.
[33] J.S. Field, Determining the Mechanical Properties of Small Volumes of Material from Submicrometer Spherical Indentations, Journal of Materials Research, 10 (1995) 101-112.
[34] B. Xu, X.Y. Wu, F. Luo, C.L. Du, X.Q. Sun, Research on the Forming Mechanism of Micro-Moulds Based on Laminated Slip-Welding of Ultrathin Stainless Steel Foils, Advanced Materials Research, 314-316 (2011) 1818-1822.
[35] S. Hou, J. Wang, X. Wang, H. Chen, L. Xiang, Effect of Mg^{2+} on hydrothermal formation of α-$CaSO_4 \cdot 0.5H_2O$ whiskers with high aspect ratios, Langmuir the Acs Journal of Surfaces & Colloids, 30 (2014) 9804.
[36] J. Zhao, Y.J. Zhu, G.F. Cheng, Y.J. Ruan, T.W. Sun, F. Chen, J. Wu, X.Y. Zhao, G.J. Ding, Microwave-assisted hydrothermal rapid synthesis of amorphous calcium phosphate nanoparticles and hydroxyapatite microspheres using cytidine 5′-triphosphate disodium salt as a phosphate source, Materials Letters, 124 (2014) 208-211.
[37] Y.P. Lu, Y.Z. Song, R.F. Zhu, M.S. Li, T.Q. Lei, Factors influencing phase compositions and structure of plasma sprayed hydroxyapatite coatings during heat treatment, Applied Surface Science, 206 (2003) 345-354.
[38] Y.P. Lu, S.T. Li, R.F. Zhu, M.S. Li, T.Q. Lei, Formation of ultrafine particles in heat treated plasma-sprayed hydroxyapatite coatings, Surface & Coatings Technology, 165 (2003) 65-70.

Table

Table 1 Detailed elastic modulus and coating hardness values of MH treated coating; MH-H-42; MH-OH-942; MH-167 and MH-0

Figure

Fig. 1 Schematic illustration of the formation of sprayed Ca-P coating and MH treated coating on C/C substrate

Fig. 2 Schematic illustration of the sprayed Ca-P coating on C/C substrate (a) and its typical high-resolution micrographs for (b) spherical particles; (c) micro-cracks; (d) holes and (e) un-melted particles

Fig. 3 FTIR spectrum (a) and (b) its high-resolution scan of the red rectangle block of sprayed Ca-P coating

Fig. 4 SEM micrographs (a) and (b), XRD pattern (c), XPS spectra (d), FTIR spectrum (e) and (f) its high-magnification of the red rectangle block of the MH treated coating

Fig. 5 SEM micrographs of sprayed Ca-P coating after treatments using H_2SO_4 solution, $NH_3 \cdot H_2O$ solution, only Ca^{2+} solution and deionized water: (a) MH-H-42; (b) MH-OH-942; (c) MH-167 and (d) MH-0

Fig. 6 XRD patterns of (a) MH-H-42; (b) MH-OH-942; (c) MH-167; (d) MH-0

Fig. 7 Mass change of the sprayed Ca-P coating and its products after treatment using MH method for MH treated coating; MH-H-42; MH-OH-942; MH-167 and MH-0

Fig. 8 XPS spectra (a) and Raman spectra (b) of MH-H-42; MH-OH-942; MH-167 and MH-0

Fig. 9 SEM micrographs for surface macrocracks of (a) sprayed Ca-P coating; (b) MH-H-42; (c) MH-OH-942; (d) MH-167; and (e) MH-0

Fig. 10 Cross-sectional micrographs of (a) MH treated coating; (b) MH-H-42 and its EDS surface map of S element (d); (c) MH-OH-942; (d) MH-167 and (f) MH-0

Fig. 11 Representative load-displacement curves from nanoindentation for MH treated coating; MH-H-42; MH-OH-942; MH-167 and MH-0

Fig. 12 Curve change of elastic modulus and hardness for the sprayed Ca-P coating; MH treated coating; MH-H-42; MH-OH-942; MH-167 and MH-0

Fig. 13 Schematic illustrations for the detailed reaction of the different solutions in the MH process: calcium and phosphorus precursor solution (Ca:P = 1.67); H_2SO_4 solution (MH-H-42); $NH_3 \cdot H_2O$ solution (MH-OH-942); only Ca^{2+} solution (MH-167) and deionized water (MH-0)

Table 1

Specimens	Elastic modulus (GPa)	Hardness (GPa)
MH treated coating	58.7 ± 6.1	3.14 ± 0.56
MH-H-42	1.5 ± 0.7	0.01 ± 0.02
MH-OH-942	51.7 ± 15.4	1.87 ± 0.99
MH-167	52.0 ± 9.5	2.80 ± 0.73
MH-0	49.2 ± 8.7	2.04 ± 0.49

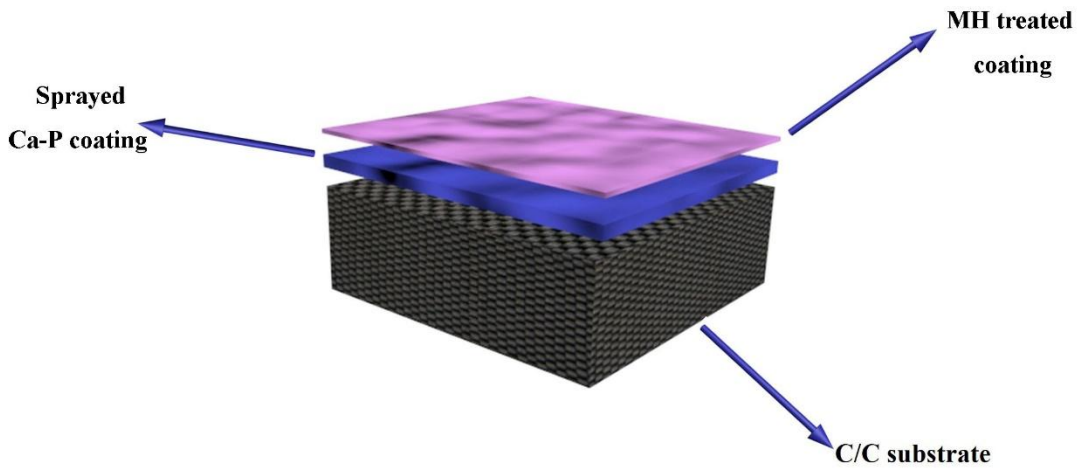

Figure 1

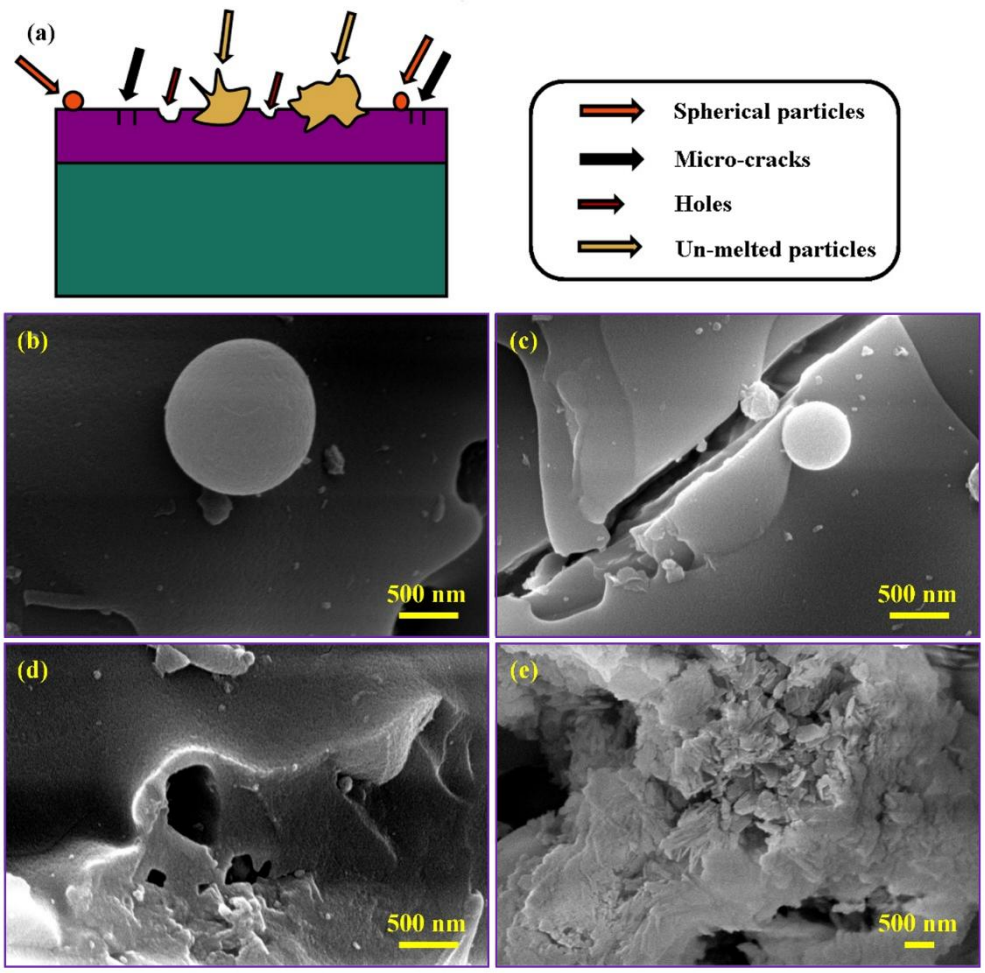
(a)
Spherical particles
Micro-cracks
Holes
Un-melted particles
(b)
500 nm
(c)
500 nm
(d)
500 nm
(e)
500 nm

Figure 2

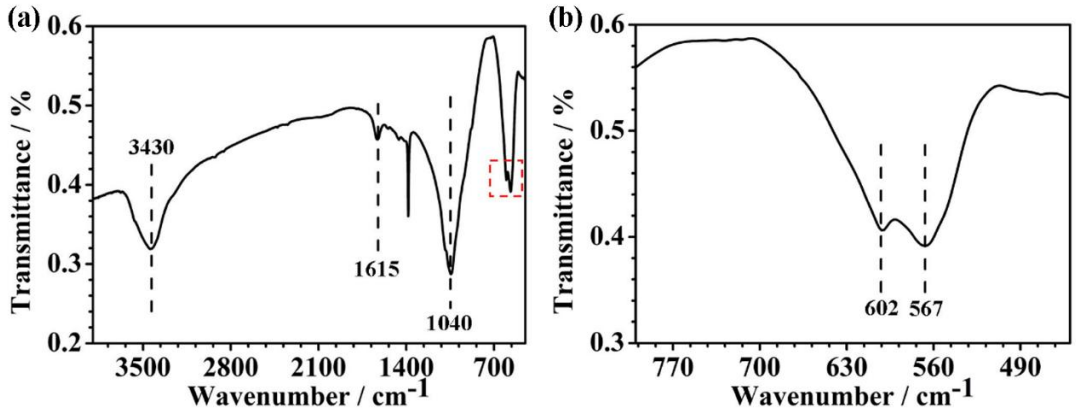
(a)
Transmittance / %
0.6
0.5
0.4
0.3
0.2
3430
1615
1040
3500
2800
2100
1400
700
Wavenumber / cm-1
(b)
Transmittance / %
0.6
0.5
0.4
0.3
602
567
770
700
630
560
490
Wavenumber / cm-1

Figure 3

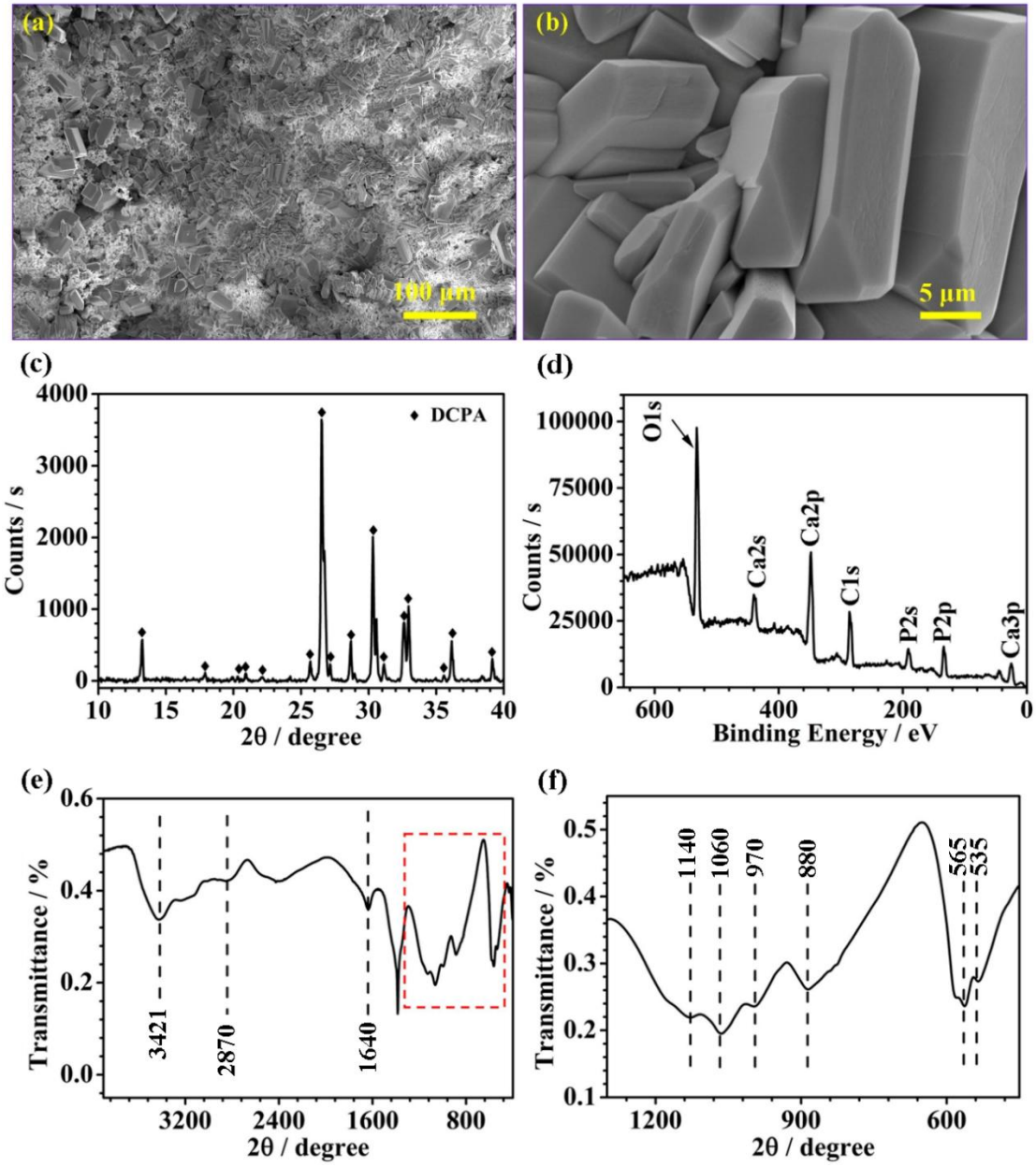
(a)
100 μm
(b)
5 μm
(c)
DCPA
Counts / s
2θ / degree
(d)
O1s
Ca2s
Ca2p
C1s
P2s
P2p
Ca3p
Counts / s
Binding Energy / eV
(e)
3421
2870
1640
Transmittance / %
2θ / degree
(f)
1140
1060
970
880
565
535
Transmittance / %
2θ / degree

Figure 4

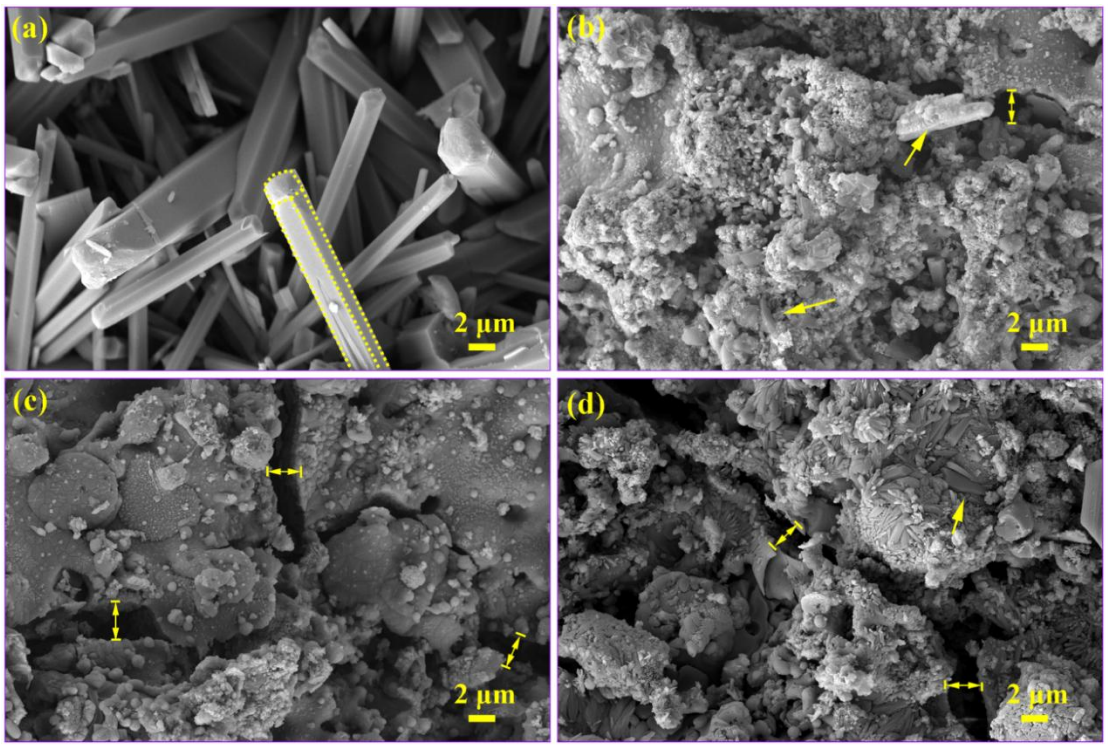

Figure 5

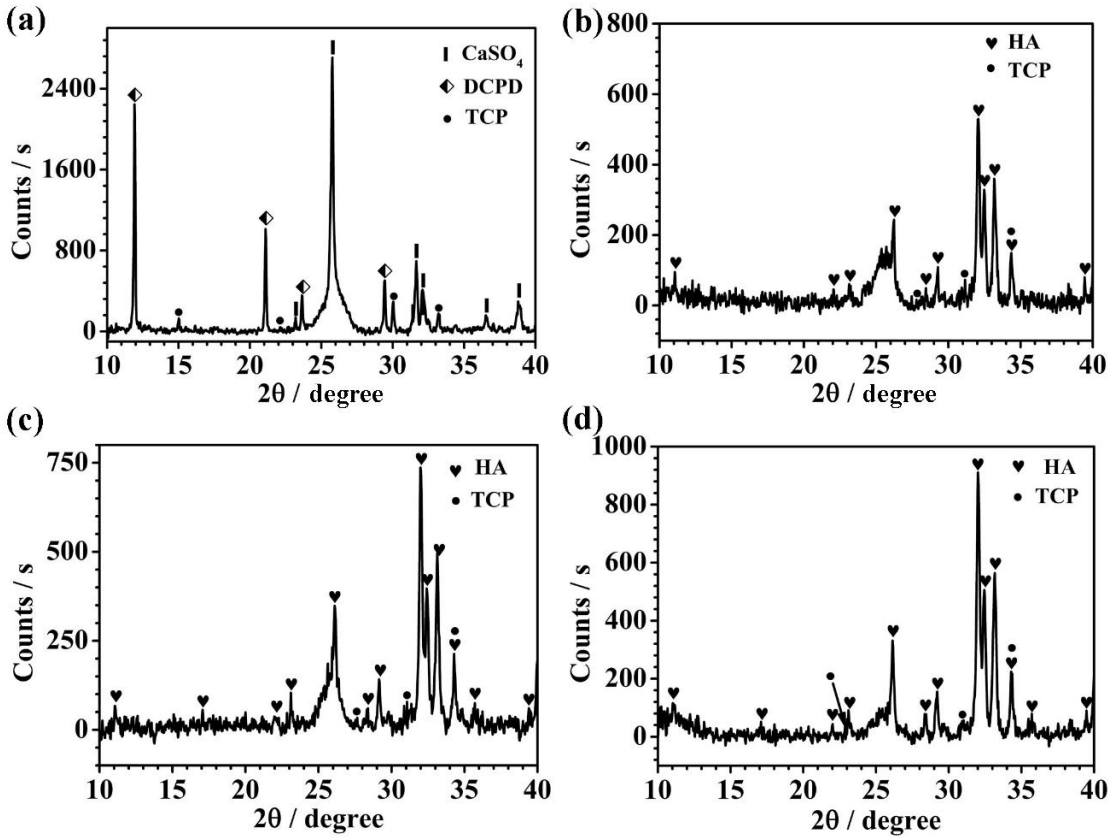
(a)
CaSO4
DCPD
TCP
Counts / s
2θ / degree
(b)
HA
TCP
Counts / s
2θ / degree
(c)
HA
TCP
Counts / s
2θ / degree
(d)
HA
TCP
Counts / s
2θ / degree

Figure 6

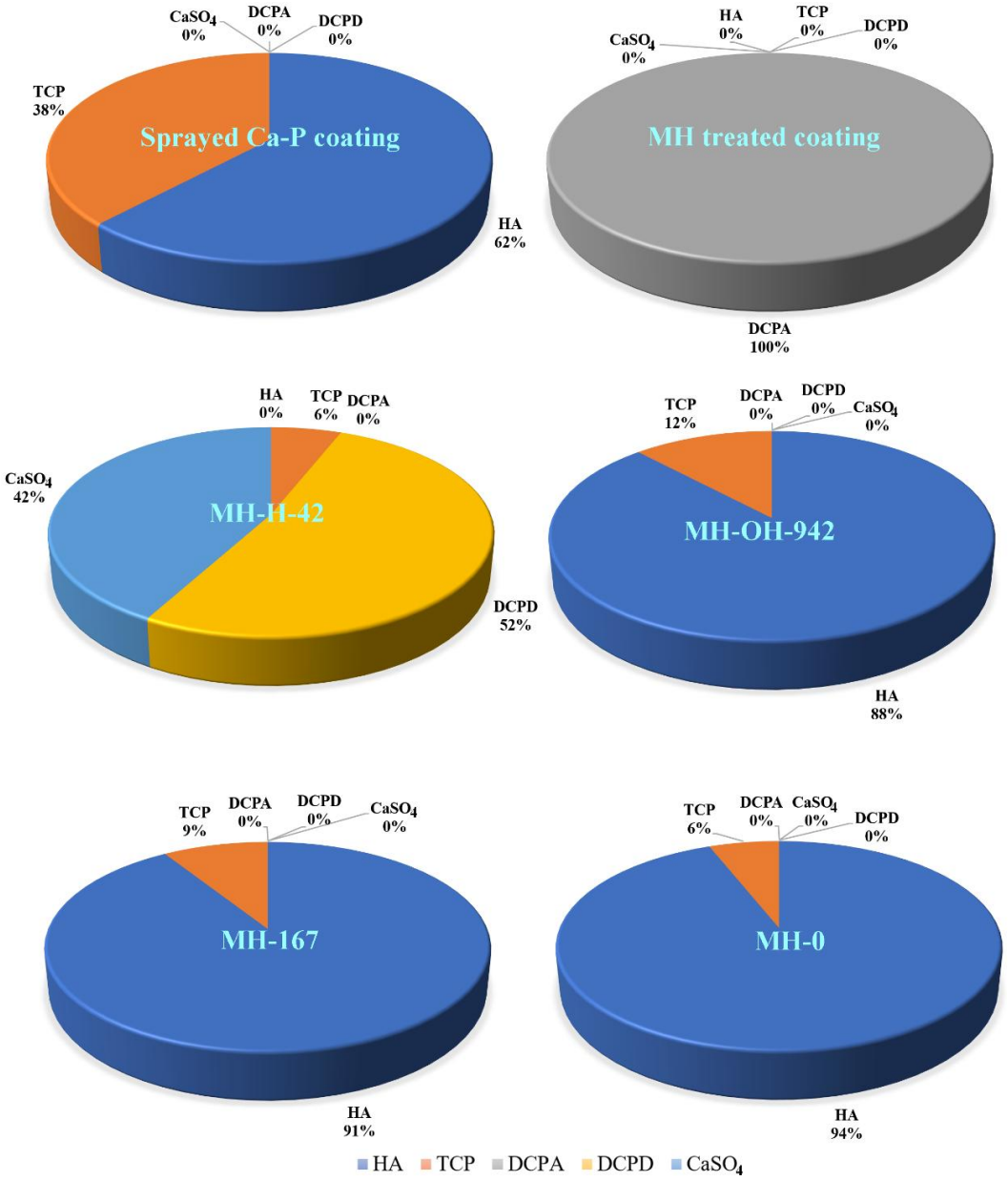
CaSO4 0%
DCPA 0%
DCPD 0%
TCP 38%
Sprayed Ca-P coating
HA 62%
HA 0%
TCP 0%
DCPD 0%
CaSO4 0%
MH treated coating
DCPA 100%
HA 0%
TCP 6%
DCPA 0%
CaSO4 42%
MH-H-42
DCPD 52%
TCP 12%
DCPA 0%
DCPD 0%
CaSO4 0%
MH-OH-942
HA 88%
TCP 9%
DCPA 0%
DCPD 0%
CaSO4 0%
MH-167
HA 91%
TCP 6%
DCPA 0%
CaSO4 0%
DCPD 0%
MH-0
HA 94%
HA
TCP
DCPA
DCPD
CaSO4

Figure 7

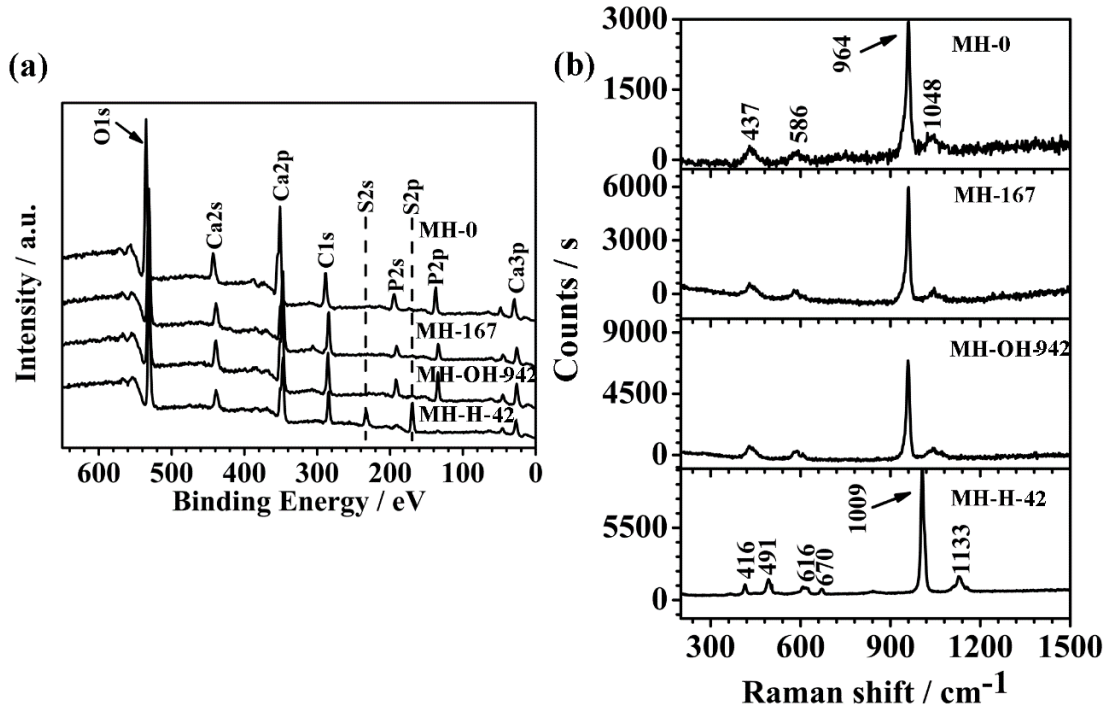
(a)
O1s
Ca2s
Ca2p
C1s
S2s
S2p
P2s
P2p
Ca3p
MH-0
MH-167
MH-OH-942
MH-H-42
Intensity / a.u.
600 500 400 300 200 100 0
Binding Energy / eV
(b)
964
437
586
1048
MH-0
MH-167
MH-OH-942
1009
MH-H-42
416
491
616
670
1133
Counts / s
3000
1500
0
6000
3000
0
9000
4500
0
5500
0
300 600 900 1200 1500
Raman shift / cm-1

Figure 8

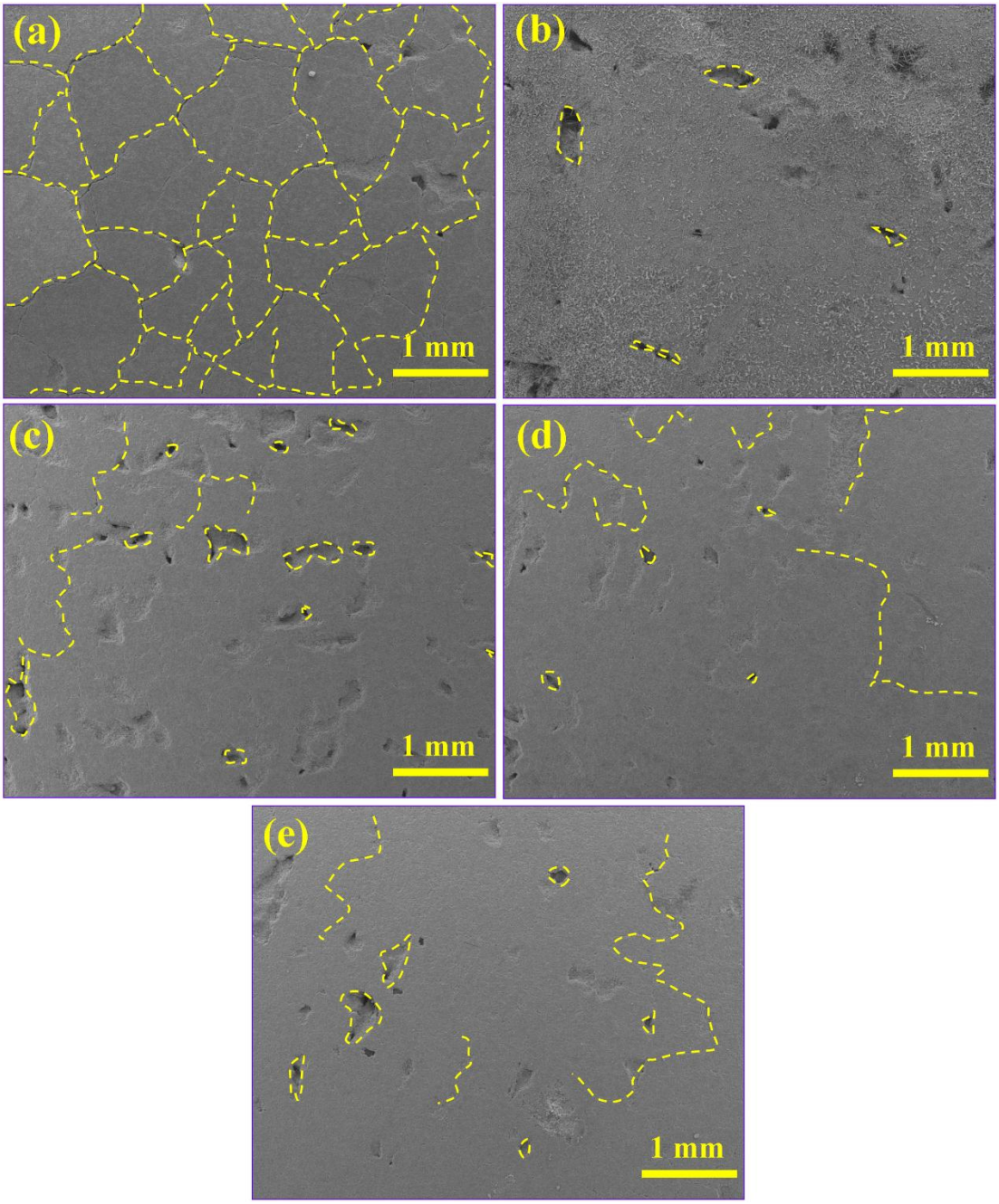

Figure 9

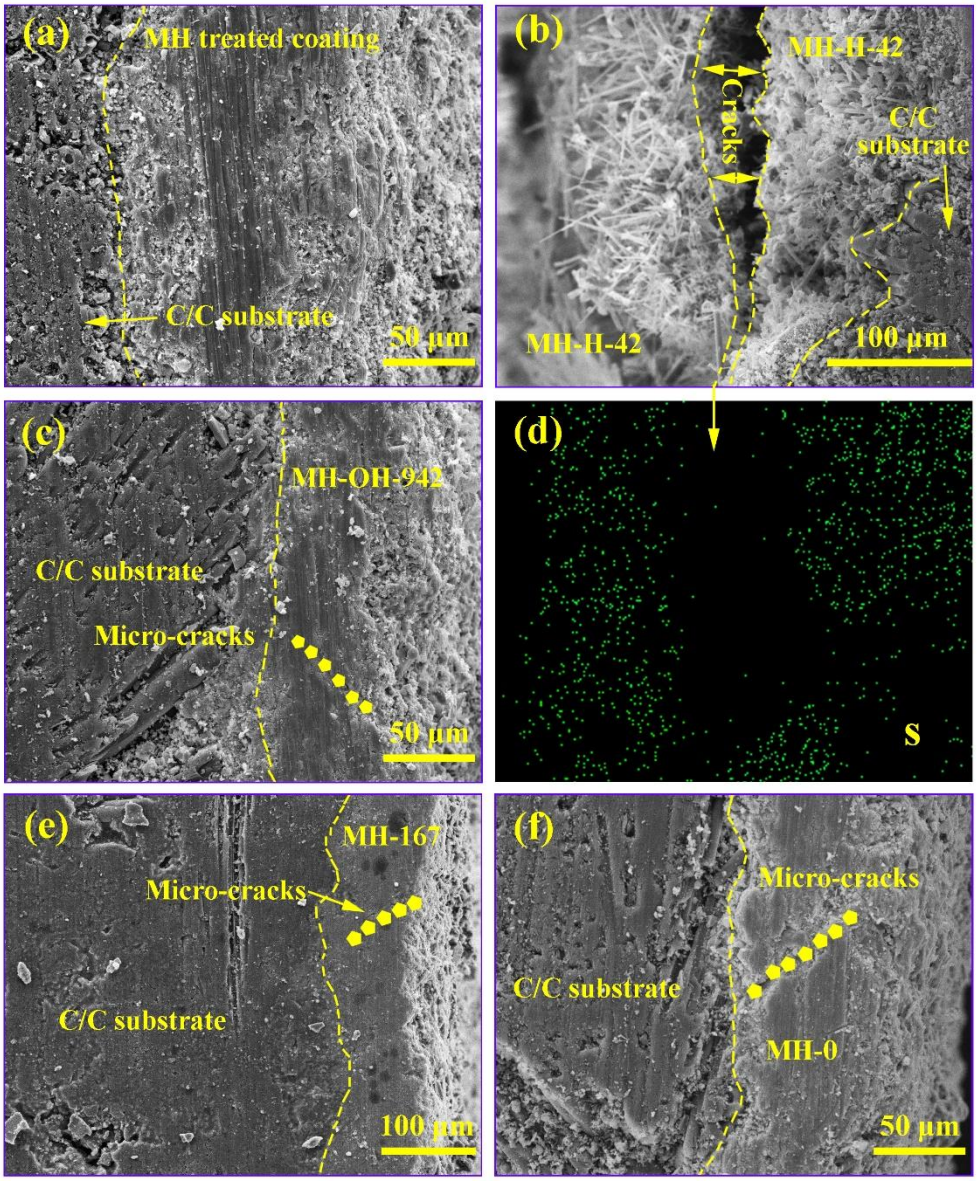
(a)
MH treated coating
C/C substrate
50 μm
(b)
MH-H-42
Cracks
C/C substrate
MH-H-42
100 μm
(c)
MH-OH-942
C/C substrate
Micro-cracks
50 μm
(d)
S
(e)
MH-167
Micro-cracks
C/C substrate
100 μm
(f)
Micro-cracks
C/C substrate
MH-0
50 μm

Figure 10

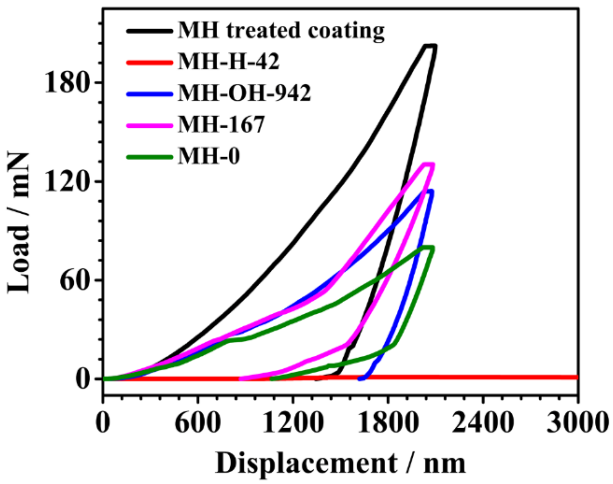
MH treated coating
MH-H-42
MH-OH-942
MH-167
MH-0
Load / mN
0
60
120
180
0
600
1200
1800
2400
3000
Displacement / nm

Figure 11

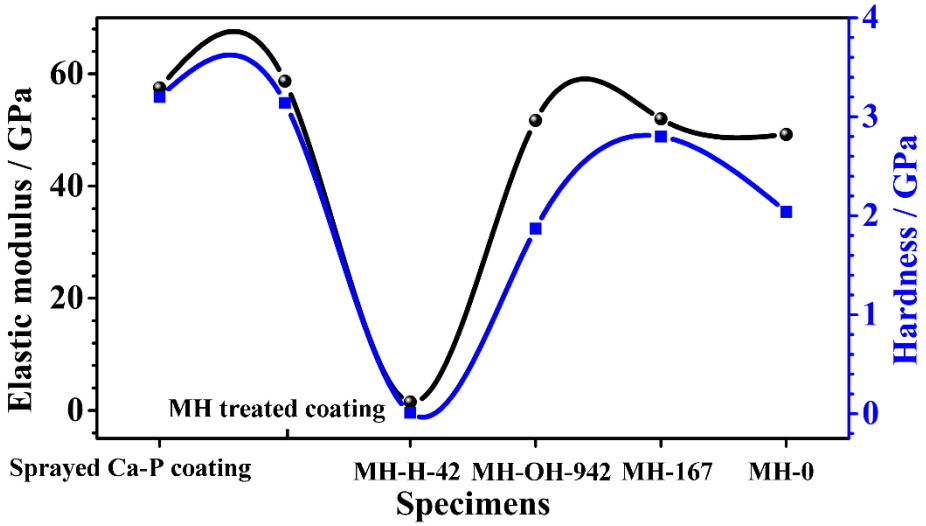
Elastic modulus / GPa
Hardness / GPa
0
20
40
60
0
1
2
3
4
MH treated coating
Sprayed Ca-P coating
MH-H-42
MH-OH-942
MH-167
MH-0
Specimens

Figure 12

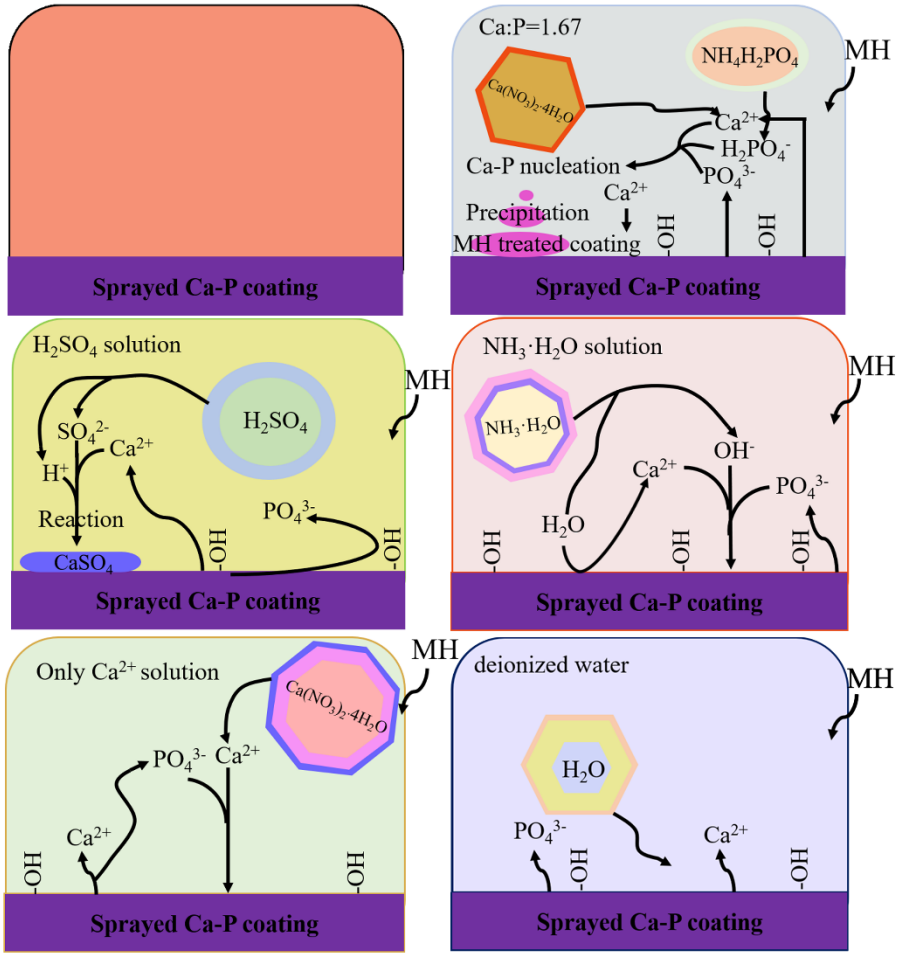
Sprayed Ca-P coating
Ca:P=1.67
$NH_4H_2PO_4$
MH
$Ca(NO_3)_2{\cdot}4H_2O$
Ca^{2+}
$H_2PO_4^-$
PO_4^{3-}
Ca-P nucleation
Precipitation
MH treated coating
-OH
H_2SO_4 solution
H_2SO_4
SO_4^{2-}
H^+
Reaction
$CaSO_4$
$NH_3{\cdot}H_2O$ solution
$NH_3{\cdot}H_2O$
OH^-
H_2O
Only Ca^{2+} solution
deionized water

Figure 13